TESTING FOR OCEANOGRAPHIC CONTROLS ON NEOGENE TEX_{86} TEMPERATURES IN THE EASTERN EQUATORIAL ATLANTIC

GEO4-1520
MSc research

Koen van der Laan
5726336

Universiteit Utrecht

1st supervisor: prof. dr. Appy Sluijs
2nd supervisor: dr. Anna von der Heydt
3rd supervisor: Carolien van der Weijst MSc
4th supervisor: dr. ir. Francien Peterse

Utrecht, July 2017

TABLE OF CONTENTS

ABSTRACT

The TEX_{86} proxy is a frequently used tool in paleoclimate studies. While TEX_{86} temperatures are often interpreted as sea surface temperatures (SSTs), the oceanographic controls on TEX_{86} are still highly debated. The input of non-locally produced isoGDGTs, enhanced activity of methanotrophic archaea, the variable production depth of isoGDGTs and/or enhanced upwelling may alter the TEX_{86} signal that is ultimately retrieved from the sedimentary archive. Here, Late Miocene to Early Pliocene TEX_{86}^{H} temperatures from the eastern equatorial Atlantic are reconstructed and tested for oceanographic controls using CCSM4 and CESM1 model output. TEX_{86}^{H} values are indicative of a more than 10 °C decrease in SST from the Late Miocene to Early Pliocene, larger than can be expected from surface water cooling alone. An abrupt fall in SST (3 °C) around 5.0 million years (Ma) marks a change in the signature of TEX_{86}. From the paleoclimate model output, I find contradictory evidence for the reinforcement of coastal upwelling at this time. While both proxy data and model output indicate a deepening and weakening of the thermocline and a strengthening of the current system, the models show no sign of excessive surface water cooling as would be expected with the onset of strong upwelling. This may suggest upwelling is not the major factor controlling TEX_{86} temperatures in the eastern equatorial Atlantic. Other processes, such as archaeal community changes, instead may underlie the change in the TEX_{86} signal.

1. INTRODUCTION

The accurate reconstruction of past variations in sea surface temperature (SST) is key in our understanding of the climate system. Over the last decades, a variety of SST-proxies has been developed, including foraminiferal $\delta^{18}O$, foraminiferal Mg/Ca ratio, $U_{37}^{K'}$ (C_{37} Unsaturated Ketone) index and TEX_{86} (TetraEther indeX of tetraethers consisting of 86 carbon atoms). The $U_{37}^{K'}$ index, first introduced by Brassel et al. (1986), is based on long-chain, unsaturated ketones, or alkenones, which are found abundantly in marine sediments (Marlowe et al., 1990). Haptophyte algae *Emiliania huxleyi* and related species from the class *Prymnesiophyceae* (Volkman et al., 1980; Marlowe et al., 1984), synthesize preferably di- or tri-unsaturated C_{37} alkenones depending on growth temperature (e.g. Conte et al., 1992; Marlow et al., 1984; Prahl & Wakeham, 1987). Previous studies have shown a linear relationship between global core-top $U_{37}^{K'}$ and mean annual SST (e.g. Conte et al., 1998; Müller et al., 1998). While the $U_{37}^{K'}$ index is a fairly robust proxy for SST, the use of the proxy is limited in settings above 28 °C, when the detection limit of tri-unsaturated alkenones is reached (Müller et al., 1998).

Schouten et al. (2002) introduced TEX_{86}, a SST proxy based on the relative distribution of isoprenoid glycerol dialkyl glycerol tetraethers (isoGDGT). isoGDGTs are archaeal membrane lipids synthesized by marine Thaumarchaeota (Brochier-Armanet et al., 2008). The number of cyclopentane moieties in these lipids has proved to increase with growth temperature and to be independent of salinity (Wuchter et al., 2004). In theory, TEX_{86} can yield temperatures as high as 39 °C (TEX_{86}^{H} calibration; Kim et al., 2010). However, the presumption that TEX_{86} reflects SST by definition has been challenged in recent years by the finding that Thaumarchaeota are nitrifiers and thus, do not depend on light as their source of energy (Wuchter et al., 2006). TEX_{86} may regionally reflect subsurface temperatures rather than SSTs (e.g. Ho & Laepple, 2016; Huguet et al., 2007; Lee et al., 2008; Lopes dos Santos et al., 2010; Seki et al., 2012). It has been suggested that the export depth of isoGDGTs is strongly related to the upwelling regime: a subsurface signal may be recorded in upwelling regions and a surface signal in non-upwelling regions (Huguet et al., 2007). However, the apparent relationship between TEX_{86} temperatures and upwelling intensity is one that is not yet fully understood and requires further research.

Ocean Drilling Program (ODP) Site 959, located in the eastern equatorial Atlantic (Fig. 1), may be of specific interest to study the oceanographic controls on TEX_{86}. The region is influenced by semiannual coastal upwelling (Verstraete, 1992) and has, over the last 20 Ma, shifted from south of the equator to north of the equator. The northward drift of Africa and/or the southward shift of the Intertropical Convergence Zone (ITCZ) may have strengthened the countercurrent system in the Gulf of Guinea and, thereby, changed the oceanographic setting (Norris, 1998). Previous work on this site by Veenstra et al. (in prep.) shows TEX_{86}^{H} SSTs of 27 to 31 °C in the Middle Miocene (13.7-11.5 Ma), consistent with our present understanding of tropical SSTs at that time (Herbert et al., 2016). TEX_{86}^{H} data by Van der Weijst et al. (in prep.), however, suggests remarkably low SSTs (20-24 °C) in the Late Pliocene (3.5-2.7 Ma). It is likely that these temperatures do not reflect SST and that, instead, the signature of TEX_{86} changed in between both periods. The documentation of the timing and rate of change and an improved understanding of the associated (oceanographic) processes would be of great value to our comprehension of the TEX_{86} proxy and its applicability in the reconstructions of past, warm climates.

The aim of this study is twofold. First, Late Miocene to Early Pliocene (11.5-3.5 Ma) $U_{37}^{K'}$ and TEX_{86} temperatures from ODP Site 959 are reconstructed. The timing and rate of SST change are discussed and compared to other tropical SST records. Second, the oceanographic changes to the eastern equatorial Atlantic between the Middle Miocene and Late Pliocene are evaluated from CCSM4/CESM1 climate model simulations in an attempt to resolve the apparent low Late Pliocene TEX_{86} temperature estimates.

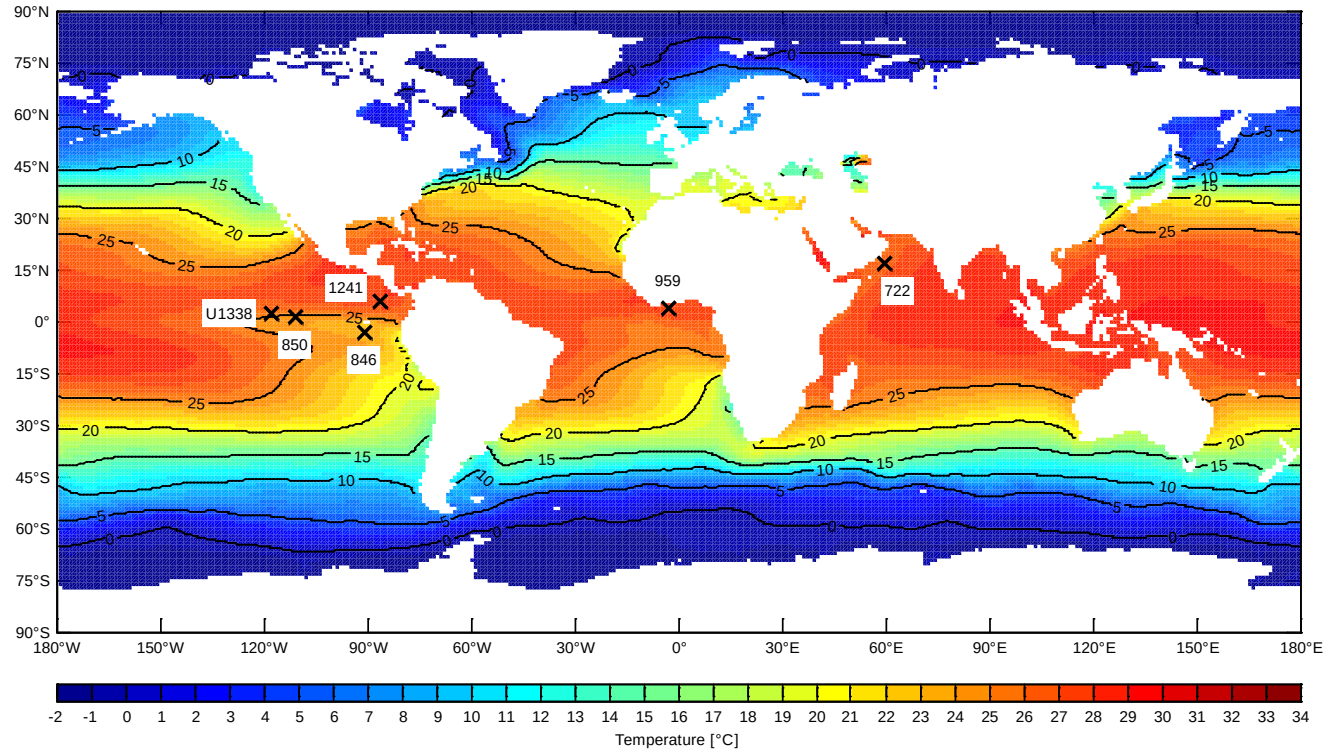

Figure 1. Ocean Drilling Program site locations used in this study superimposed on a modern SST map (National Oceanic and Atmospheric Administration; www.ospo.noaa.gov)

2. BACKGROUND INFORMATION

2.1. Neogene climate

2.1.1. Late Miocene to Early Pliocene climate evolution

In the long-term cooling trend, the Mid-Miocene Climatic Optimum (MMCO; ca. 17-15 Ma) represents one of the last warm periods of the Neogene. Notwithstanding relatively modest atmospheric pCO_2 (350-400 ppmv; Beerling & Royer, 2011; Foster et al., 2012), benthic foraminiferal oxygen isotope ($\delta^{18}O$) data indicates well-above-modern temperatures in the deep ocean (ca. 4-5 °C; Zachos et al., 2001). Relative to the present-day, the climate system was characterized by dramatically elevated SSTs in mid-to-high latitudes (You et al., 2009), a reduced latitudinal temperature gradients, a deep equatorial thermocline (LaRiviere et al., 2012), a reduced extent of the East Antarctic ice sheet (Flower & Kennett, 1994) and an intensified hydrological cycle (Bruch et al., 2011). The reestablishment of ice sheets on Antarctica between ca. 14.1-13.8 Ma (Lewis et al., 2008) imposed large-scale changes to the climate system and ecosystems that culminated in the Late Miocene (ca. 11.6-5.3 Ma). Marine SST records are indicative of modest cooling prior to 7.2 Ma, with North Atlantic SSTs still 17 °C above modern conditions in the Late Serravalian to Early Tortonian interval (ca. 12-11 Ma; Herbert et al., 2016). With no significant shifts in pCO_2 (200-260 ppmv; Beerling & Royer, 2011; Foster et al., 2012; Pagani et al., 1999), progressive cooling of mid-to-high latitudes in the Messinian (7.2-5.3 Ma) brought SSTs to near-modern values. Notably, SSTs in the tropics only cooled moderately during the Late Miocene. The period concurs with the first evidence for brief glaciations in the Northern Hemisphere (Larsen et al., 1994) and an increase of the equator-to-pole temperature gradient. On land, the onset of rapid aridification of the subtropics ca. 8 Ma ago and the vast expansion of C_4 grasslands (using the C_4 photosynthetic pathway) in favor of C_3 plants at tropical to subtropical latitudes (Cerling et al., 1997; Dupont et al., 2013), coincided with major turnovers in terrestrial fauna (Wang et al., 1994). In the Early Pliocene (5.3-2.6 Ma), climate temporarily returned to a more equable state, with above-modern temperatures throughout most of the Pliocene.

2.1.2. Uplift and closure of the Central American Seaway

The Late Cenozoic uplift and final closure of the Central American Seaway (CAS) is one of the key features of Neogene climate evolution and is thought to have resulted in a major reorganization of ocean circulation and an alteration of Northern Hemisphere climate (Keigwin, 1982; Maier-Reimer et al., 1990). Most notably, a reduced mixing of Atlantic and Pacific water masses and an increased poleward salt and heat transport would have promoted deep water formation in the subpolar North Atlantic and strengthened the Atlantic thermohaline circulation (Haug et al., 2001; Steph et al., 2006). It has been suggested that the subsequent enhancement of evaporation rates and intensified moisture flux to the northern (sub)polar region, was a precondition for ice-sheet growth that triggered the onset of Northern Hemisphere Glaciation (NHG; 3.2-2.7 Ma) (Bar-

toli et al., 2005; Haug & Tiedemann, 1998; Keigwin, 1982; Lunt et al., 2008). The precise timing of final CAS closure and the critical width and depth of the seaway required to affect interoceanic circulation (Lunt et al., 2008; Sepulchre et al., 2014), however, are still highly debated. While most paleoceanographic proxy records indicate that final closure of the CAS was established between 4.6-3.6 Ma (e.g. Groeneveld et al., 2008; Haug & Tiedemann, 1998; Haug et al., 2001; Steph et al., 2006), land-based geologic evidence suggests an earlier (19-13 Ma) isolation of the Atlantic and Pacific basin (Kirby et al., 2008; Montes et al., 2015).

2.1.3. Model-data mismatches

The use of model-data comparisons is a popular, yet intricate tool in paleoclimate studies. Mismatches between proxy and model data are usually complex and can often not be ascribed to a single cause. Limitations in the physics and structure of models, uncertainties in the interpretation of proxy records and limitations in the experimental design of models, complicate model-data comparisons (Haywood et al., 2013). This is particularly true for climatic periods of increased warmth, such as the MPWP and MMCO, that are characterized by above-modern temperatures in mid-to-high latitudes and near-modern atmospheric pCO_2 concentrations (ca. 400 ppmv) (Zachos et al., 2008). Climate models typically underestimate proxy-derived global MAT and overestimate the equator-to-pole temperature gradient (Rosenbloom et al., 2013; Goldner et al., 2014). Model-data mismatches are most explicit in the subpolar North Atlantic, where proxy-derived temperatures exceed model estimates by as much as 10 °C. Typically, only experiments that are forced with unrealistically high pCO_2 can achieve results comparable to proxy records.

The precise effects of model-data mismatches in high latitudes on the interpretation of low-latitude oceanographic data are not easily confined. The present inability of climate models to reconstruct the reduced meridional temperature gradient observed in proxy records, however, is likely to sort effect on the equatorial region. Notably, a reduced equator-to-pole SST gradient would imply a vast poleward expansion of the tropical warm pool (Brierley et al., 2009). This, in turn, would lead to a slowdown of the atmospheric Hadley circulation, prevailing El Niño-like conditions in the tropics due to a reduction in the equatorial SST gradient, a deepening of the east-west tropical thermocline (Boccaletti et al., 2004; Fedorov et al., 2004) and a weakening of wind-driven upwelling (Fedorov et al., 2013). The fact that model-data mismatches in the equatorial region are typically small may be a false positive, and hence, model data should be interpreted carefully. This may be particularly true for studies involving the seasonal cycle, due to the tight linkage of seasonality in the equatorial region to the climatic state of the extratropics. Studies of long-term climate evolutions, however, may still provide valuable results.

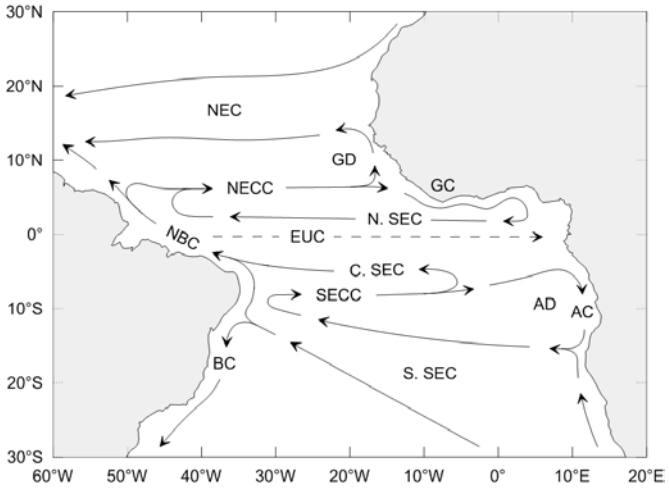

Figure 2. Schematics of the equatorial Atlantic current system. NEC = North Equatorial Current; NECC = North Equatorial Counter Current; GC = Guinea Current (GC); N. SEC = "North" South Equatorial Current; C. SEC = "Central" South Equatorial Current; S. SEC = "South" South Equatorial Current; SECC = South Equatorial Counter Current; AG = Angola Current; NBC = North Brazil Current; BC = Brazil Current; EUC = Equatorial Undercurrent; GD = Guinea Dome; AD = Angola Dome. Solid (dashed) lines indicate surface (subsurface) currents. Figure after Talley (2011).

2.2. Regional oceanography

The equatorial Atlantic current system is wind-driven and responds strongly to the easterly trade winds (30°S to 30°N) (Talley, 2011). Although the current system is similar to that of the Pacific, circulation is typically weaker due to the narrow width of the Atlantic basin. The main (near) surface flow within 15° of the equator is westward and for a large part concentrated in the South Equatorial Current (SEC; Fig. 2), which can be subdivided into a southern, central and northern component. The south SEC (sSEC) is the westward to northwestward flow in the most northern part of the South Atlantic's subtropical gyre, that originates in the Benguela Current at the southern tip of Africa. At the western boundary, it bifurcates into the Brazil Current (BC) to the south and the North Brazil Current (NBC) to the north. The equatorial part of the SEC, the central SEC (cSEC; 4-6°S) and north SEC (nSEC; 2-4°N), is bounded to the north by the North Equatorial Counter Current (NECC). The NECC (5-7°N) is directed eastward and associated with the ITCZ wind forcing. It splits southwest of Western Africa into a northward flow and the eastward Guinea Current (GC). The GC follows the African coastline, turns south and then joins the North SEC and upwelled waters that originate from the Equatorial Undercurrent (EUC). The northward flow turns eastward between 10-15°N to join the North Equatorial Current (NEC), that forms the southernmost part of the North Atlantic's subtropical gyre. The cyclonic movement of the surface currents produces an upwelling center known as the Guinea Dome, a region of pronounced upwelling and great primary productivity. At 7-8°S, the seasonally present South Equatorial Counter Current (SECC), associated with the southern displacement of the ITZC, flows eastward. Upwelled waters from the EUC join the SECC near the African coast. The SECC then turns

south, forming the Angola Current (AC), and westward around 15°S to join the South SEC, enclosing a cyclonic upwelling region known as the Angola Dome. At the equator, the trade winds produce an eastward pressure gradient that drives the eastward flowing EUC. It originates at >100 m depth near the Brazilian coast and gradually shoals to approximately 30 m depth at the eastern boundary.

2.3. Seasonality and mechanisms for coastal upwelling

Seasonality over Gulf of Guinea is largely controlled by the annual latitudinal migration of the ITCZ that shifts from 5-10°N in February to 15-20°N in August (Binet & Marchal, 1993; Gu & Adler, 2004). Mainly due to the prevailing low pressure system over Western Africa, southwesterly monsoonal winds are prevalent in the Gulf of Guinea (Roy, 1995). Wind stress is highest in boreal summer (~30 m^2/s^2), when the African monsoon system is most intense and frequent rainfall occurs over the Sahel region (Sultan & Janicot, 2003), and lowest in boreal winter (~10 m^2/s^2). Seasonal upwelling, marked by strong surface water cooling and abundant biological productivity in the surface ocean, occurs primarily along the African coast between 8°W and 2°E, from Cape Palmas (Côte d'Ivoire) to Cotonou (Benin) (Picaut, 1983). The surface water cooling tends to be strongest on the concave coasts east of Cape Palmas and Cape Three Points (Ghana) and is most pronounced from June to October. A secondary upwelling event of shorter duration and lower intensity occurs from January to February. SSTs vary between 27-29 °C outside of upwelling seasons to 22-24 °C during the major upwelling event (Hardman-Mountford & McGlade, 2003; Jouanno et al., 2011; Roy, 1995).

In subtropical eastern boundary current systems, such as the Canary Current System and Benguela Upwelling System, located off northwest and southwest Africa respectively, the seasonal coastal upwelling results largely from equatorward (upwelling favorable) wind stress that promotes Ekman divergence at the coast (Bakun & Nelson, 1991). In the Gulf of Guinea, however, Ekman-type wind-driven upwelling cannot explain a significant part of the upwelling along the northern coast of the Gulf of Guinea (Bakun, 1978; Houghton, 1976). Also, the east-west rather than north-south orientation of the coast and the westward propagation of the upwelling event against the flow of the Guinea Current (Picaut, 1983) differentiate the Gulf of Guinea from other eastern boundary current systems. Other dynamical processes that have been proposed for coastal upwelling in the Gulf of Guinea include (1) the coastal shallowing of the thermocline through the interaction between the Guinea Current and Cape Palmas and Cape Three Points (Marchal & Picaut, 1977), (2) the coastal shallowing of the thermocline by the geostrophic adjustment to an intensification of the Guinea Current (Ingham, 1970), (3) enhanced vertical mixing due to increased vertical shear at the base of Guinea Current as a result of an intensification of the Guinea Current (Jouanno et al., 2011) and (4) an increase of the zonal (westward) wind stress in the western equatorial Atlantic and the associated excitement of an internal upwelling Kelvin wave that propagates eastward along the equator and reflects as (westward) coastal Kelvin and Rossby waves at the eastern boundary (Moore et al., 1978). However, none of the above mechanisms has yet been able to fully explain the upwelling events in the Gulf of Guinea. Therefore, coastal upwelling is probably a product of a combination of both remote and local forcings (Roy, 1995).

2.4. TEX_{86} temperatures

2.4.1. Relevant calibration models

The initial core-top calibration model introduced by Schouten et al. (2002) is based on the relative distribution of GDGT-1, GDGT-2 and GDGT-3, representing isoGDGTs with 1, 2 and 3 cyclopentane moieties respectively, and the regio-isomer of crenarchaeol, containing 4 cyclopentane moieties and 1 cyclohexane moiety:

$$TEX_{86} = \frac{[GDGT-2]+[GDGT-3]+[Cren']}{[GDGT-1]+[GDGT-2]+[GDGT-3]+[Cren']} \quad (1)$$

Schouten et al. (2002) showed a linear relationship between TEX_{86} value and mean annual SST based on a relatively small core-top dataset (n = 44). The calibration was updated using a more extensive, global core-top dataset (n = 284) by Kim et al. (2008). Likewise, they found a linear correlation of TEX_{86} with SST between 5 to 30 °C. Over the full core-top temperature range (-2 to 30 °C), however, the relationship was found to be non-linear, largely due to the minor changes in TEX_{86} with temperature below 5 °C. Kim et al. (2010) analyzed an additional 116 core-top samples from the sub(polar) oceans to improve the spatial coverage of the global core-top dataset (n = 426) and proposed two new indices and calibration models, named TEX_{86}^{L} and TEX_{86}^{H}, based on their findings. TEX_{86}^{L} is a modified version of TEX_{86} with a logarithmic function, which excludes the regio-isomer of crenarchaeol. In (sub)polar oceans, the role of the regio-isomer of crenarchaeol in the membrane adaptation of Thaumarchaeota to temperature seems limited. Therefore, it was suggested that TEX_{86}^{L} is most applicable in low-temperature environments. Conversely, the role of the regio-isomer of crenarchaeol in the temperature adaptation of Thaumarchaeota seems to be much larger in sub(tropical) and past "greenhouse world" oceans. TEX_{86}^{H} (eq. 2 and 3), defined as the logarithmic function of TEX_{86}, yields more reliable SST predictions in these high-temperature environments. Kim et al. (2010) recommended use of the TEX_{86}^{H} calibration in settings above 15 °C.

$$TEX_{86}^{H} = \log \frac{[GDGT-2]+[GDGT-3]+[Cren']}{[GDGT-1]+[GDGT-2]+[GDGT-3]+[Cren']} \quad (2)$$

$$SST = 68.4 \times TEX_{86}^{H} + 38.6 \quad (3)$$

Tierney & Tingley (2014) recently introduced the BAYSPAR (BAYesian SPAtially-varying Regression) calibration model. They argued that, regardless of the functional form or the choice of data, all other calibration models feature residual patterns indicative of a tendency to overestimate SSTs at high-latitude sites and underestimate SSTs at low-latitude sites. BAYSPAR allows regression parameters that link TEX_{86} and SST to vary as a function of space. The "standard" version of the model draws regression parameters from the model grid point (20° × 20°) nearest to the core site. The "deep-time" version, best used to infer SSTs in time periods where Earth's continental configuration and climatic state were different from today, searches the core-top calibration dataset for TEX_{86} values that are similar to those in the time series and then draws the regression parameters from these analogue sites. Using this method, the residual bias is reduced and uncertainty estimates become more meaningful. SSTs in regions with fewer core-top samples or that are dependent on the extrapolation of the calibration are featured with larger uncertainty bounds. Likewise, uncertainties increase in "deep-time" applications, when regression parameters are typically drawn from multiple analogues sites.

2.4.2. Origin of the TEX_{86} signal

While TEX_{86} is often interpreted as a proxy for mean annual SSTs, TEX_{86} values may regionally reflect a deeper and/or cooler water mass (Chen et al., 2014; Ho & Laepple, 2016; Huguet et al., 2007; Lee et al., 2008; Lopes dos Santos et al., 2010; Rommerskirchen et al., 2011; Seki et al., 2012). Thaumarchaeota, the primary producers of isoGDGTs in the marine realm, are distributed throughout the water column and can reside in deeper waters (Karner et al., 2001) relative to alkenone-producing haptophyte algae, which can only thrive in the euphotic zone (Müller et al., 1998). In times of ammonium scarcity, Thaumarchaeota may be outcompeted by phytoplankton and forced to thrive at depths or seasons less favorable to alkenone producers (Lee et al., 2008; Pitcher et al., 2011; Turich et al., 2007; Wuchter et al., 2006). While isoGDGTs have indeed been reported to be most abundant below the surface mixed layer (>100 m) (Wuchter et al., 2005), it is thought that upwelling is key in the transport of these cold-biased isoGDGTs to the sediments; it seems that in non-upwelling regions, the TEX_{86} signal is still primarily derived from the surface mixed layer (Sinninghe Damsté et al., 2002; Wakeham et al., 2004). The (seasonal) upwelling of cold, nutrient-rich water is thought to increase biological productivity in the surface ocean (Huguet et al., 2006; Lee et al., 2008; Wuchter et al., 2006). This would increase the amount of marine snow and fecal pellet production and promote the export of isoGDGTs produced at depth or potentially even upward advected "cold" isoGDGTs to the ocean floor through packaging. This is supported by observations that fluxes of isoGDGTs are seasonal and highest during upwelling (Herfort et al., 2006; Huguet et al., 2007; Wakeham et al., 2002; Wuchter et al., 2005).

2.4.3. Branched and Isoprenoid Tetraether (BIT) index and Methane Index (MI)

TEX_{86} values in coastal areas may be biased by the input of fluvially transported isoGDGTs. These land-based isoGDGTs originate mainly from wetland environments, such as peats (Pancost et al., 2000; Schouten et al., 2000; Weijers et al., 2004), and are likely produced by methanogenic archaea (Pancost et al., 2000). The relative input of land-based isoGDGTs into the marine realm can be approximated by the ratio between so-called branched GDGTs (bGDGTs), containing branched instead of isoprenoid alkyl chains, and crenarchaeol in the Branched and Isoprenoid Tetraether (BIT) index (eq. 4; Hopmans et al., 2004). The index is based on the fact that (1) crenarchaeol is particularly abundant in the marine environment and its relative contribution via fluvial transport is small and (2) bGDGTs, which are presumed to be of bacterial origin, are predominant in terrestrial environments, such as peats and soils (Sinninghe Damsté et al., 2000; Weijers et al., 2006). The ratio between the two endmembers can hence be used to determine the relative contribution of terrestrial organic matter and, indirect, land-based isoGDGTs to the marine environment. BIT index values range from 0 to 1. Low values correspond to high relative abundances of crenarchaeol, which indicate the predominance isoGDGTs produced in the marine realm. High values denote the predominance of terrestrially-produced isoGDGTs. BIT values below 0.3 generally yield trustworthy TEX_{86} values (Weijers et al., 2006).

$$BIT = \frac{[GDGT-Ia]+[GDGT-IIa]+[GDGT-IIIa]}{[GDGT-Ia]+[GDGT-IIa]+[GDGT-IIIa]+[Cren]} \quad (4)$$

In gas hydrate and/or methane-rich deep sea environments, an alternative bias may be introduced to TEX_{86} by methanotrophic (methane-oxidizing) archaea, which preferentially produce isoGDGTs with 1 to 3 cyclopentane moieties (GDGT-1, GDGT-2 and GDGT-3) as their membrane lipid (Blumenberg et al., 2004). In order to quantify the relative contribution of methanotrophic archaea versus Thaumarchaeota (crenarchaeol and its regio-isomer) to GDGT distributions, the Methane Index (MI) was developed (eq. 5; Zhang et al., 2011). MI values range from 0 to 1. Low values correspond to high fractional abundances of GDGT-1, GDGT-2 and GDGT-3, which may indicate the predominance of methane-oxidizing archaea. High values indicate the predominance of non-methanotrophic Thaumarchaeota. MI values below 0.3 generally yield reliable TEX_{86} values.

$$MI = \frac{[GDGT-1]+[GDGT-2]+[GDGT-3]}{[GDGT-1]+[GDGT-2]+[GDGT-3]+[Cren]+[Cren']} \quad (5)$$

2.4.4. Archaeal community changes

Recent studies have observed an increase of GDGT-2 relative to GDGT-3 in suspended particulate matter and surface sediments with increasing water depth (Hernández-Sánchez et al., 2014; Taylor et al., 2013). The authors argued that an elevated ratio of GDGT-2 to GDGT-3 (hereafter referred to as [2]/[3] ratio) may be related to an increased contribution of Thaumarchaeota living in deeper waters. Kim et al. (2015) noticed a strong positive relationship between water depth and TEX_{86}^{H} due to increased fractional abundances of GDGT-2 and the region-isomer of crenarchaeol and lower fractional abundances of GDGT-1 and GDGT-3 in deeper waters, which resulted in a warm bias towards TEX_{86}^{H} values. The above led to the suggestion that the changing [2]/[3] ratio may result from a change in the Thaumarchaeotal community that thrives below the surface mixed layer. From a paleoceanographic point of view, the [2]/[3] ratio may hence be used to reconstruct changes in Thaumarchaeota populations over time.

3. MATERIAL

3.1. Study location

Site 959 of Ocean Drilling Program (ODP) Leg 159 is located in the Gulf of Guinea, the northeasternmost part of the equatorial Atlantic (3°37.669'N, 2°44.116'W; 2102 m water depth; Fig. 1). It forms part of an extensional margin, known as the Deep Ivorian Basin, that extends north of the Cote d'Ivoire-Ghana Marginal Ridge. The Neogene sedimentary succession primarily consists of clayey pelagic and hemipelagic oozes and chalks, containing vast amount of nanofossils and foraminifers (Mascle et al., 1996).

3.2. Age model

The age model is largely based on high-resolution X-Ray Fluorescence (XRF) data by Vallé et al. (2016). Here, iron (Fe) intensity data from ODP Site 959 Hole A, B and C was used to construct a composite depth record (22.64-109.25 rmcd). The cyclic patterns in the depth domain were then orbitally tuned to develop a highly-detailed age model from 6.2-1.8 Ma. To this end, the major cycle in the record (2 m) was tuned to the short eccentricity cycle (100 ky). Shorter cycles (1 m, 0.5 m and 0.4 m), only expressed from 52 rmcd to the base of the record, were tuned to the obliquity cycle (1 m) and the mean precession cycle (0.5 m and 0.4 m). No strong shifts were found in the period bands of the wavelet spectra, indicating rapid changes in sedimentation rate did not occur in the studied interval. In order to date the sediments below the depth interval studied by Vallé et al. (2016), linear interpolation between the last cyclostratigraphic tie point and the first of some biostratigraphic tie points (13.5-11.5 Ma) by Veenstra et al. (in prep) was used.

3.3. The Community Climate System Model and Community Earth System Model

3.3.1. General characteristics

The Community Climate System Model version 4 (CCSM4) and its successor, the Community Earth System Model version 1 (CESM1), are fully-coupled, state-of-the-art General Circulation Models (GCMs) that consist of atmosphere, land surface, ocean and sea ice components that are interlinked through a coupler (Gent et al., 2011). They provide highly detailed simulations of past, present and future climate states and are typically used in IPCC climate projections. The ocean component is based on the Parallel Ocean Program version 2 (POP2; Smith et al., 2010) that uses a displaced-pole ocean grid, with the poles in Greenland and Antarctica. The horizontal grid has 320×384 points with a resolution of 1.11° in the zonal direction and 0.27° to 0.54° in the meridional direction. The vertical grid consists of 60 levels, including twenty 10 m levels in the upper ocean.

3.3.2. Preindustrial control

An 1850 preindustrial (PI) control run (Rosenbloom et al., 2013), conducted with version 4 of the CCSM conform CMIP5 (Coupled Model Intercomparison Project Phase 5) protocols (Taylor et al., 2012), may be used as a reference to modern climate. The PI control was run for 1300 years and forced with modern boundary conditions and constant pCO_2 (284.7 ppmv). Results show a global mean annual temperature (MAT) of 14.0 °C, global mean SST of 20.4 °C and an Atlantic Meridional Overturning Circulation (AMOC) of 26 Sv. The equator-to-pole temperature gradients are 13.4 °C and 11.1 °C in the Northern Hemisphere and Southern Hemisphere respectively.

3.3.3. Mid-Pliocene Warm Period

One 500-year CCSM4 simulation of the MPWP (Rosenbloom et al., 2013; hereafter referred to as Experiment 1) is used to study Late Pliocene climate. It was conducted as part of the initial phase of the Pliocene Model Intercomparison Project (PlioMIP), Experiment 2 (Haywood et al., 2011), and the larger Paleoclimate Modelling Intercomparison Project (PMIP). The forcings and boundary conditions, including vegetation, topography, SST and sea/land ice cover were prescribed from version 3 of the Pliocene Research, Interpretation and Synoptic Mapping project (PRISM3; Dowsett et al., 2010). Ocean bathymetry and the continental configuration remained largely unaltered from the PI control. The atmospheric pCO_2 was set to 405 ppmv, similar to present-day values, and kept constant throughout the experiment. Results show a 1.9 °C increase in glob-

al mean annual temperature (MAT) relative to the PI control and a polar amplification of ca. 3 times the global mean warming. SSTs in the eastern equatorial Pacific warm by 1-2 °C, thereby reducing the zonal SST gradient and weakening the El Niño-Southern Oscillation (ENSO). The northward ocean heat transport in the Atlantic and strength of the AMOC are virtually identical to the PI control.

3.3.4. Middle Miocene

Two CESM (version 1.0.5.) atmosphere-ocean simulations of the Middle Miocene (Herold et al., in prep.; hereafter referred to as Experiment 2a and 2b) are used as a reference to Miocene climate. Both simulations were run for 2000 years and forced with Miocene vegetation, topography and bathymetry and constant atmospheric pCO_2 (400 ppmv). Different to the preindustrial and Late Pliocene continental configuration, the Central American Seaway (CAS) was opened. Results show a weakened overturning circulation due to reduced deep water formation in the North Atlantic. To simulate the effects of North Atlantic ventilation, the Canadian Archipelago (CA) was opened to a depth of 30 m in one of the experiments (Experiment 2b). While the latter is not the aim of this study, the effects of increased North Atlantic ventilation on the tropical climate are interesting to discuss.

4. METHODS

4.1. Geochemical analysis

For this study, 76 samples from the 50-160 m interval of ODP Site 959 hole C, covering the late Miocene to early Pliocene (~11.2-3.8 Ma) were analyzed. Sediment samples were retrieved from the IODP Bremen Core Repository in Bremen, Germany, and analyzed at the GEOLAB at Utrecht University in Utrecht, the Netherlands. On arrival in Utrecht, the samples were freeze-dried and temporarily stored. First, each sample was finely crushed and extracted (ca. 5 g) with a Dionex Accelerated Solvent Extractor 350, using a 9:1 dichloromethane (DCM)/methanol solvent mixture. Solvents in the total lipid extract (TLE) were evaporated using a Caliper Life Sciences TurboVap LV. The TLE was then separated into an apolar, ketone and polar fraction via alumina column chromatography, using 9:1 hexane/DCM, 1:1 hexane/DCM and 1:1 DCM/methanol solvent mixtures respectively. A C_{46} GDGT (99 ng) standard was added to the polar fraction to later quantify GDGT abundances. Solvents were again evaporated from the vials and each fraction was subsequently weighted. The polar fraction was then dissolved in a 300 µl solvent mixture of 99:1 hexane/isopropanol, filtered through a 0.45 µm polytetrafluoroethylene (PTFE) membrane filter and analyzed with Ultrahigh-Performance Liquid Chromatography-Mass Spectrometry (UHPLC-MS; method according to Hopmans et al., 2016) Prior to each sequence, a reference standard with a known amount of C_{46} GDGTs was run to prevent calibration issues. GDGT peak areas were integrated manually and converted into SST using the TEX_{86}^{H} (eq. 2-3; Kim et al., 2010) and BAYSPAR calibration models (Tierley & Tingley, 2014) (for details see 2.4.1.). In the latter calibration, the "deep time" version was used along with the default settings.

The ketone fraction was dissolved in 100-500 µl ethyl acetate proportional to the weight of the fraction (ca. 100 µl/0.2 mg) and analyzed using Gas Chromatography (GC). 1 µl of sample was injected using an auto-sampler. Ketone peak areas were integrated manually and converted into SST as described by Müller et al. (1998):

$$U_{37}^{K'} = \frac{[C_{37:2}]}{[C_{37:2}]+[C_{37:3}]} \quad (5)$$

$$SST = \frac{U_{37}^{K'} - 0.044}{0.033} \quad (6)$$

4.2. Climate model data

The climate model data of the PI control run and MPWP simulation was downloaded from the Earth System Grid at the National Center for Atmospheric Research (ESG-NCAR; www.earthsystemgrid.org). To reduce errors due to temporal variability, data was averaged over the last 10 years of each run. Herold et al. (in prep.) provided 50-year averages of the Middle Miocene simulations. Data was processes and analyzed using MATLAB R2013a.

5. RESULTS

5.1. Neogene SST record

Sedimentary material from ODP Site 959 was analyzed to establish a new eastern equatorial Atlantic SST-record for the Late Neogene (ca. 11.2-3.8; Fig. 3a). TEX_{86}^{H} values in the compiled record (this study; Van der Weijst et al., in prep.; Veenstra et al., in prep.) suggest a more than 10 °C decrease in SSTs from 12.8-2.7 Ma. SSTs approximate 31 °C from 12.8-11.5 Ma and gradually cool by roughly ca. 3.5 °C over the next 2.5 Ma (ca. 1.4 °C/Ma). A brief phase of modest warming (9.0-8.5 Ma) shortly interrupts the long-term cooling trend. SSTs continue to cool gradually from 8.5-5.0 Ma by an additional 2.5 °C (ca. 0.7 °C/Ma) and average 25.5 °C around 5.0 Ma. In the last 0.5 Ma of this interval (5.5-5.0 Ma), the record shows increased variability. SSTs then quickly fall to 23.5-24.0 °C in less than 0.2 Ma and remain relatively stable from 4.8-3.7 Ma. Progressive cooling (ca. 4 °C) is continued over the next 1.6 Ma (3.7-3.0 Ma) and is only briefly intermitted by a period of sustained warmth (ca. 3.3-3.0 Ma). In the 4.8-3.0 Ma interval, variability is typically high. Past 3.0 Ma, SSTs gradually warm to roughly 23 °C at 2.6 Ma. The BAYSPAR calibration model (Fig. 3a) has the same trend as the TEX_{86}^{H} record described above, but shows an even larger decrease in SST from 11.2 (33.2 °C) to 3.8 Ma (22.7 °C).

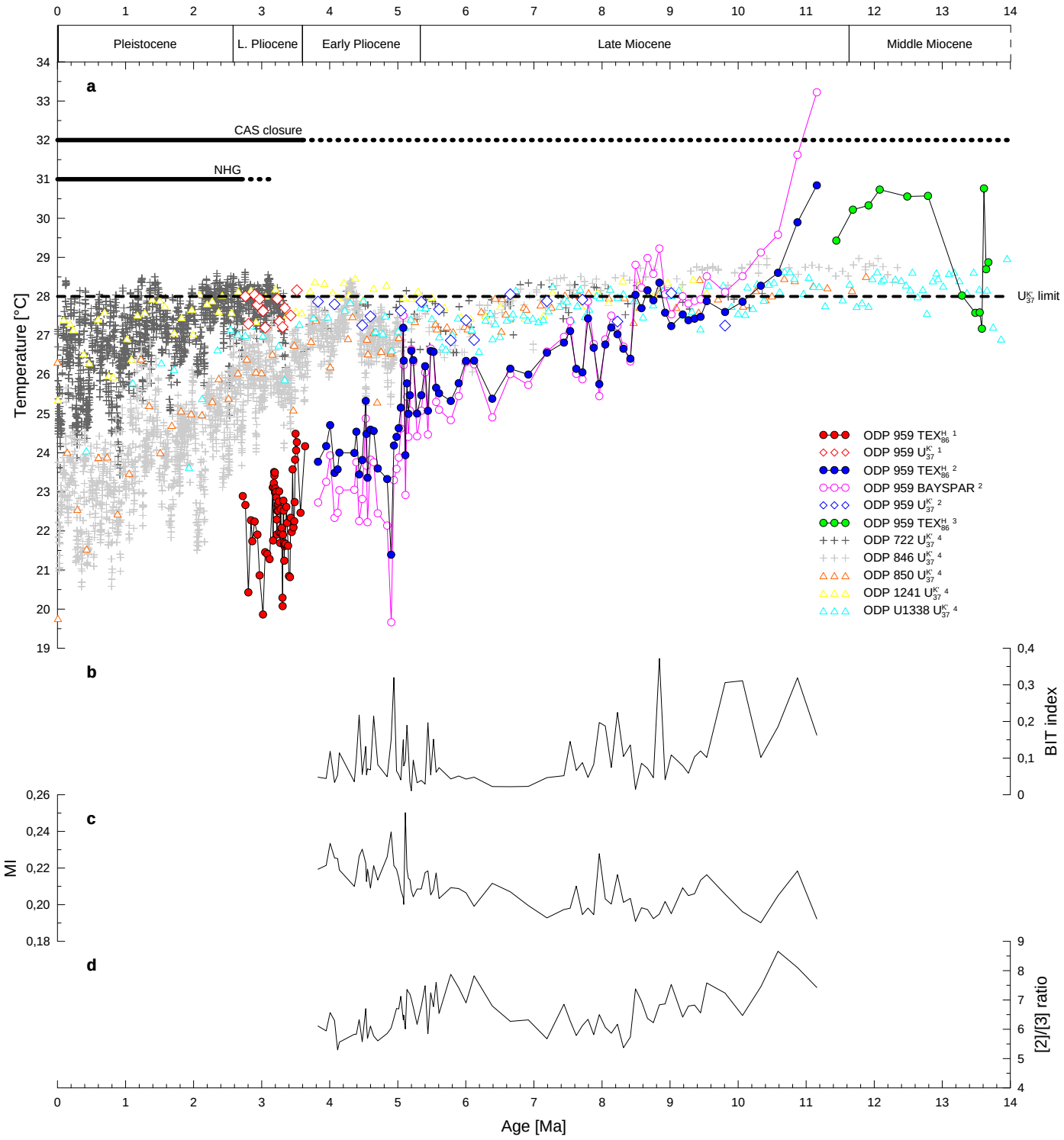

Figure 3. a. SST evolution over the past 14 Ma. Records include the data presented in this study[2] and data by Van der Weijst et al. (in prep.)[1], Veenstra et al. (in prep.)[3] and Herbert et al. (2016) and references therein[4]. The dashed line at 28 °C represents the $U^{K'}_{37}$ calibration limit. Timing of the final closure of the Central American Seaway (CAS) and Northern Hemisphere Glaciation (NHG) are indicated as solid/dotted lines. **b-d.** BIT index, Methane Index (MI) and the GDGT-2 to GDGT-3 ratio for the analyzed samples of ODP Site 959.

The reconstructed $U^{K'}_{37}$ temperatures all plot between 26.6 and 28.1 °C (Fig. 3a). It is likely, however, that most of the samples reached the calibration limit of the $U^{K'}_{37}$ proxy. The authenticity of the reconstructed SSTs is hence difficult to assess. Nevertheless, it is obvious that TEX^{H}_{86} yields consistently lower temperatures than $U^{K'}_{37}$ from ca. 8.0-2.6 Ma. The offset is largest around 3.0 Ma, where $U^{K'}_{37}$ and TEX^{H}_{86} SSTs deviate by as much as 8 °C.

5.2. BIT index and MI

The vast majority (71 out of 76) of the analyzed samples have BIT index values below 0.3 (Fig. 3b). Since the outliers only have slightly higher BIT index values (0.31-0.37) and linear regression analyses show no significant correlation between both BIT index and age (R^2 = 0.11) and BIT index and TEX^{H}_{86} temperatures (R^2 = 0.06), all samples were included in the TEX_{86} record. MI values (Fig.

3c) all plot between 0.19 and 0.25, well below the cutoff value.

5.3. GDGT-2 to GDGT-3 ratio

The [2]/[3] ratio (Fig. 3d) is highest in the earliest part of the record. In the 11.2-7.2 Ma interval, values gradually decrease from 8.6 to 5.7. The ratio then steadily increases over the next 1 Ma to 7.8 at 6.2 Ma and again is indicative of a decreasing trend from 6.2-5.0 Ma. Here, values decrease only slightly from 7.8 to 6.7. The ratio then slightly drops and averages 5.7 past 5.0 Ma. Variability is high over the entire record.

5.4. Thermal structure of the upper ocean

The thermal structure of the upper 250 m of the ocean around ODP Site 959 is described to evaluate changes in the depth and strength of the thermocline. To reduce errors due to spatial variations, temperatures are averaged over a 5×5° area surrounding ODP Site 959 (Fig. 4c). The size of the area was determined as the largest area possible without a significant influence of other water masses.

Mixed layer (35 m) temperatures approximate 28.2 °C in Experiment 1 (Fig. 4a). Below the mixed layer, temperatures rapidly decrease with depth to ca. 16 °C around 110 m and remain relatively stable from 110-160 m. From 160-250 m, waters cool by an additional 4 °C. The vertical temperature gradient, often used as an indication for thermocline depth, reaches maximum values of 0.3 °C/m around 55 m depth (Fig. 4b). The thermal structure of the PI control resembles that of the Experiment 1. Although the latter has considerably higher temperatures (0.5-1.5 °C) at every depth, the vertical temperature gradients are virtually identical. Experiment 2a and 2b are notably different from the PI control and Experiment 1. Here, mixed layer depth is 25 m, with temperatures that approximate 30.8 °C (Experiment 2a) and 30.4 °C (Experiment 2b). Over the next 85 m, temperatures quickly fall by 12-13 °C. Cooling is most intense at 40-45 m depth with maximum values of 3.2 °C/m and 3.6 °C/m for Experiment 2a and 2b respectively. Below 110 m, waters cool more gradually (0.02-0.04 °C/m) to approximately 15 °C (Experiment 2a) and 14 °C (Experiment 2b) around 250 m depth.

Summarizing, Experiment 2a and 2b are typified by a more shallow (ca. 10 m) and intense (0.2-0.6 °C/m) thermocline relative to the PI control and Experiment 1. Opening of the CA in Experiment 2b has no major effects on the depth of the mixed layer, but does slightly weaken the thermocline.

5.5. Zonal velocities in the eastern equatorial Atlantic current system

The currents in the equatorial Atlantic are mainly zonal (Fig. 5; Supplementary Fig. 1). Eastward surface flow (0-30

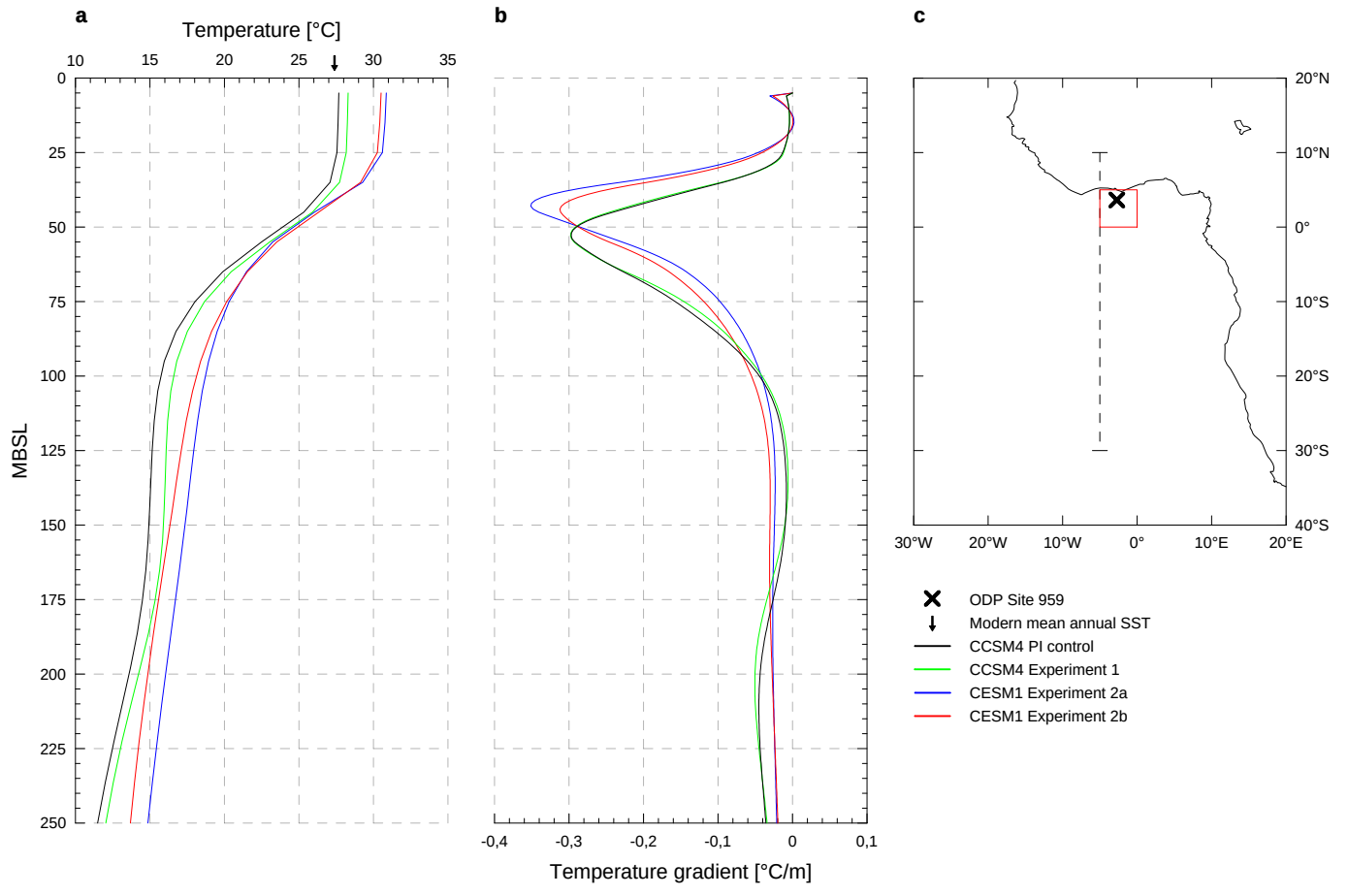

Figure 4. a. Thermal structure of the upper ocean (250 m) around ODP Site 959 **b.** Vertical temperature gradient **c.** Map of site location. The red box indicates the 5×5° area over which temperatures were averaged. The dashed line indicates the cross section which was used for Supplementary Fig. 1.

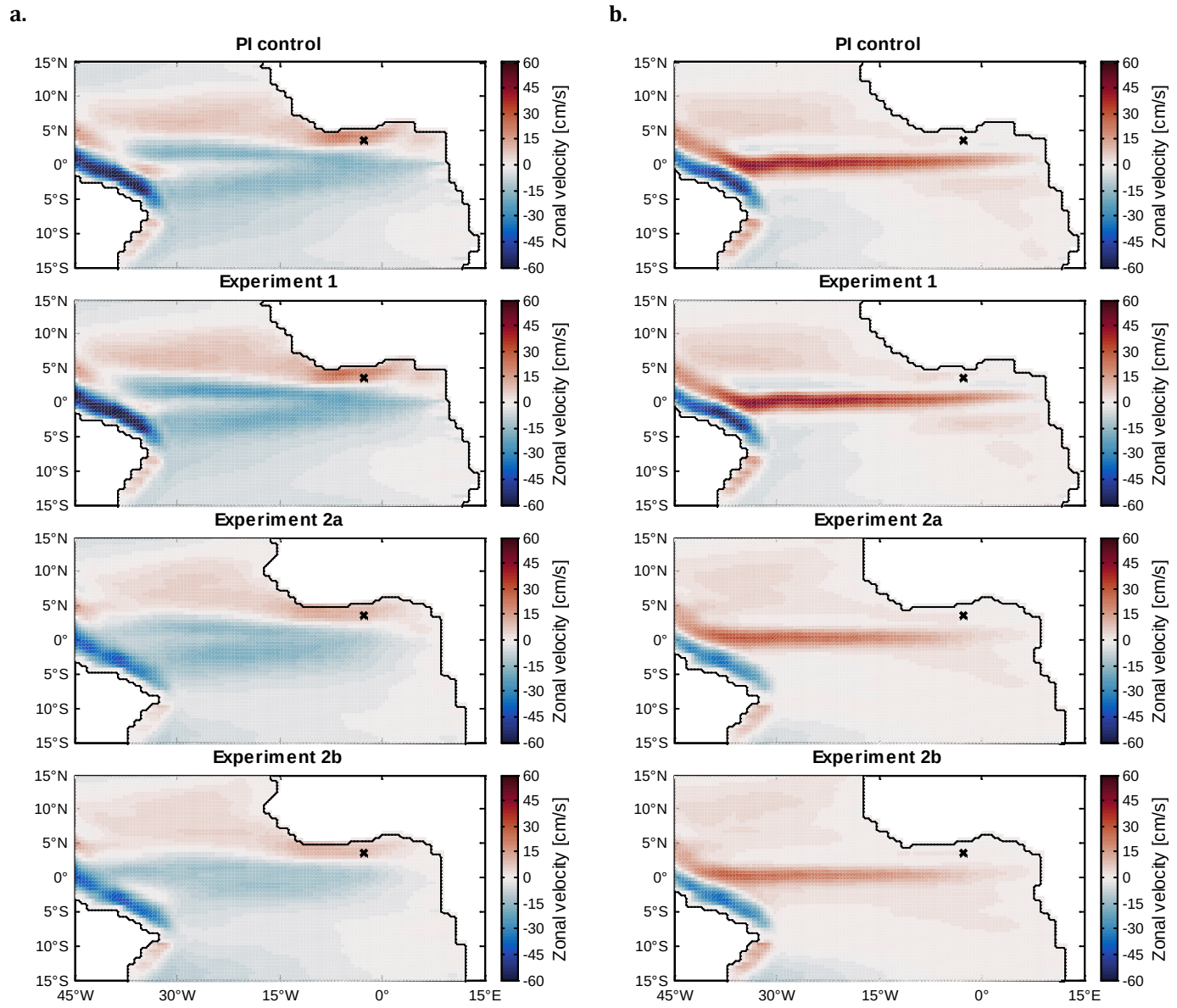

Figure 5. Zonal velocities in the equatorial Atlantic averaged over **a.** 0-30 m depth. **b.** 30-150 m depth. Red (blue) colors indicate an eastward (westward) flow. The black cross indicates the location of ODP Site 959.

m depth) is concentrated in the NECC (5-10°N). Zonal velocities in the NECC are relatively low in the western Atlantic, where transport occurs over a broad region; zonal velocities nearly double southwest of Western Africa, where the NECC narrows and merges into the GC (2-5°N) that transport water into the Gulf of Guinea. Westward surface flow occurs mainly south of 2°N in the SEC. Here, waters flow over a broad region with zonal velocities that are similar to those observed in the GC. Subsurface flow (30-130 m depth) is concentrated in the EUC, that flows at the equator with velocities 4-5 times as high as in the NECC. In terms of absolute zonal velocities, the PI control and Experiment 1 very much resemble each other (Table 1): velocities are highest in the EUC and lowest in the NECC; the GC and SEC are comparable in strength. In Experiment 2a and 2b zonal velocities are in general 1.5-2 times as low as in the PI control and Experiment 1. Opening of the CA in Experiment 2b has no major effects on the strength of the currents. Notably, all experiments do not show any obvious shifts in the position of the (sub)surface currents; the effects are solely expressed in the strength of the NECC, GC, SEC and EUC.

	PI control	Exp. 1	Exp. 2a	Exp. 2b
NECC	10	11	7	6
GC	26	28	15	14
SEC	-20	-27	-19	-14
EUC	48	48	33	31

velocities in cm/s

Table 1. Maximum zonal velocities in the (sub)surface currents of the eastern equatorial Atlantic, inferred from CCSM4/CESM1 paleoclimate models. Positive (negative) values indicates eastward (westward) flow.

6. DISCUSSION

6.1. Neogene SST evolution in the eastern equatorial Atlantic

The Neogene SST record at ODP Site 959 (Fig. 3a) can roughly be subdivided into three parts: (1) a phase (12.8-

5.0 Ma) of prolonged, relatively modest cooling with above-modern SSTs, (2) a short phase (5.0-4.8 Ma) of intense cooling and (3) a second phase (4.8-2.6 Ma) of more modest cooling, typified by increased SST variability and below-modern SSTs. In explaining the pattern of SST change at ODP Site 959, various processes should be considered.

Surface water cooling is very likely to have contributed to the decrease in SST at ODP Site 959. Possibly the best reference to the Late Neogene tropical SST evolution is provided by Herbert et al. (2016). Reconstructed Late Neogene (12.0-2.7 Ma) $U^{K'}_{37}$ SSTs for the eastern equatorial Atlantic and Arabian Sea (Fig. 3a) are indicative of a gradual 3-4 °C cooling of surface waters. Even though cooling may have been slightly more progressive, due to the maximization of $U^{K'}_{37}$ values and the (presumable) underestimation of SSTs prior to 8 Ma, it is unlikely that SST change in the tropics was as high as surface water cooling in mid-to-high latitudes (ca. 10-15 °C; Herbert et al., 2016). Regarding the more than 10 °C decrease in TEX^{H}_{86} SST at ODP Site 959, it is therefore unlikely that the full SST change over the Late Neogene was due to surface water cooling. It may however, provide an explanation for the earliest part of the TEX^{H}_{86} record (12.8-5.0 Ma), where the rate of SST change is roughly similar to the tropical mean decrease in SST and absolute SSTs fall within calibration error of TEX^{H}_{86} (2.5 °C; Kim et al., 2008). The subsequent fall in SST from 5.0 to 4.8 Ma, however, can impossibly be due to surface water cooling alone. Both the magnitude and rate of change suggest a sudden change to the TEX_{86} signal.

The initiation or reinforcement of (seasonal) upwelling may provide an explanation for the remarkably low TEX^{H}_{86} temperatures after 5.0 Ma . Indications for upwelling variability in the Gulf of Guinea have previously been studied by Norris (1998). Here, the $\delta^{18}O$ values of surface (*G. sacculifer*) and subsurface dwelling foraminifera (*N. dutertrei* and *G. margaritae*) were used to reconstruct the thermal gradient in the upper ocean. Typically, regions with a thick mixed layer and deep thermocline, such as the western Atlantic, produce small $\delta^{18}O$ gradients between these species (ca. 0.6-0.7 ‰; Ravelo & Fairbanks, 1992), which is about half of that found in the eastern Atlantic. Intriguingly, upwelling systems also tend to produce small $\delta^{18}O$ gradients, as both surface and subsurface species thrive in the same upwelled water. In these regions, the thermocline typically weakens and SSTs are depressed. The 1.5 ‰ decrease in $\delta^{18}O$ gradient at ODP Site 959 5.2 and 4.5 Ma ago (Supplementary Fig. 2b), equivalent with a drop in temperature of as much as 7 °C, can thus be interpreted as either a deepening or a weakening of the thermocline. Norris (1998) concluded that the true adjustment of the thermocline was likely a combination of both and interpreted the change in $\delta^{18}O$ gradient as the shift from a strongly stratified water column before 4.5 Ma to a slightly deeper and weaker thermocline afterwards. He and Billups (1999) ascribed the change to a reduced influence of the SEC due to an intensification of the GC. Regions that are influenced by the SEC, such as today's offshore Gabon, have an intense, shallow thermocline where upwelled waters typically do not reach into the surface mixed layer. In contrast, GC-dominated regions, such as the modern Gulf of Guinea, usually show a deeper and weaker thermocline. Here, upwelled waters do seasonally reach to the surface. Mechanisms that have been related to an intensification of the GC include the northward drift of the African continent and a southward shift of the ITCZ, which is thought to be related to the Late Cenozoic tectonic uplift of the CAS (Billups, 1999). The notion that increased upwelling was induced by the closure of the CAS has already gained support by previous studies conducted in the eastern equatorial Pacific (Ibaraki, 1997; Kamikuri et al., 2009).

6.2. Indications for upwelling variability inferred from model data

To test whether upwelling is likely to have intensified from 5.0 Ma onward, the oceanographic data from Experiment 1 and Experiment 2a and 2b is used. The most obvious dissimilarity between both experiments is the presence of the CAS. What part of the oceanographic changes can directly be related to the closing/opening of the CAS, however, is difficult to assess. Nonetheless, Experiment 1 is indicative of a clear strengthening of the overturning circulation relative to Experiment 2a and 2b. In the eastern equatorial Atlantic, this is expressed in an intensification of the current system (Fig. 5; Table 1). The increase of zonal velocities and the subsequent geostrophic adjustment of the GC may have promoted coastal upwelling in the northern Gulf of Guinea. However, Experiment 1 does not register an excessive cooling of surface waters, as would be expected with the onset of intensified (seasonal) upwelling. Instead, surface water cooling is roughly equal to the tropical mean decrease in SST (ca. 2.2 °C). This may suggest the adjustment of the thermocline was more a deepening rather than a weakening and, hence, would oppose the intensification of upwelling. The thermal structure around ODP Site 959 (Fig. 4) indeed indicates a deepening of the thermocline in Experiment 1 relative to Experiment 2a and 2b as proposed by Norris (1998), but the decrease in temperature gradient between the surface mixed layer and thermocline is surely not as high as the decrease in $\delta^{18}O$ gradient would suggest (ca. 7 °C). The latter is particularly true for Experiment 2b, where the change in thermal structure is only expressed in a deepening of the thermocline.

From the paleoclimate models, there are hence no obvious indications for the onset of unusual strong upwelling in the Gulf of Guinea. Ideally, I would have studied the seasonal cycle, as upwelling in the Gulf of Guinea is a semiannual phenomenon. The present limitations in paleoclimate models, however, prevent such detailed studies. Therefore, other proxies, such as the diol index, which is based on the relative abundance of long-chain 1,14-alkyl diols produced by *Proboscia* diatoms (Rampen et al., 2008), may be used to study upwelling variability in the Gulf of Guinea. Lastly,

also the importance of biological changes to the TEX_{86} signal should be further evaluated. The [2]/[3] ratio presented here (Fig. 3d) is indicative of a shift around 5.0 Ma, but further research is needed to assess whether the observed shift is significant and truly reflects an archaeal community change.

7. CONCLUSION

Here, I presented a new Late Neogene SST record for the eastern equatorial Atlantic. TEX_{86}^{H} temperatures decrease by more than 10 °C from 13.7 to 2.7 Ma and yield consistently lower values than $U_{37}^{K'}$-based SSTs from 5.0 Ma onward, when TEX_{86}^{H} temperatures abruptly fall by ca. 3 °C. The rate and magnitude of SST change are unmatched in other tropical SST records, suggesting surface water cooling alone cannot explain the full temperature change. Instead, it is likely that the signature of TEX_{86} changed significantly around 5.0 Ma. I find no evidence for the unusual high input of terrestrially-produced isoGDGTs (BIT index) or high input of isoGDGTs produced by methane-oxidizing archaea (MI). Previous suggestions that upwelling in the eastern equatorial Atlantic was intensified due to the uplift of the Central American Seaway, are only partially supported by the climate model data used in this study. The models are indeed indicative of a weakening and deepening of the thermocline and an intensification of the Guinea Current, but show no sign of excessive surface water cooling as would be expected with the onset of strong (seasonal) upwelling. The present inability of paleoclimate models to correctly reproduce the seasonal cycle, however, may cause misinterpretation. Upwelling in the Gulf of Guinea is seasonal and may not be expressed in the multidecadal averages that were compiled for this study. Therefore, for the near future, additional proxy-based research and season-resolving modeling is needed to be able to constrain Neogene upwelling variability in the Gulf of Guinea. Further, more research is needed to evaluate the importance of archaeal community changes to TEX_{86} values.

REFERENCES

Bakun, A. (1978). Guinea current upwelling. Nature, 271(5641), 147-150.

Bakun, A., & Nelson, C. S. (1991). The seasonal cycle of wind-stress curl in subtropical eastern boundary current regions. Journal of Physical Oceanography, 21(12), 1815-1834.

Bartoli, G., Sarnthein, M., Weinelt, M., Erlenkeuser, H., Garbe-Schönberg, D., & Lea, D. W. (2005). Final closure of Panama and the onset of northern hemisphere glaciation. Earth and Planetary Science Letters, 237(1), 33-44.

Beerling, D. J., & Royer, D. L. (2011). Convergent cenozoic CO2 history. Nature Geoscience, 4(7), 418-420.

Blumenberg, M., Seifert, R., Reitner, J., Pape, T., & Michaelis, W. (2004). Membrane lipid patterns typify distinct anaerobic methanotrophic consortia. Proceedings of the National Academy of Sciences of the United States of America, 101(30), 11111-11116.

Billups, K., Ravelo, A. C., Zachos, J. C., & Norris, R. D. (1999). Link between oceanic heat transport, thermohaline circulation, and the Intertropi cal Convergence Zone in the early Pliocene Atlantic. Geology, 27(4), 319-322.

Binet, D., & Marchal, E. (1993). The large marine ecosystem of shelf areas in the Gulf of Guinea: long-term variability induced by climatic changes. Large Marine Ecosystems: Stress, Mitigation, and Sustainability, 104-118.

Brassell, S. C., Eglinton, G., Marlowe, I. T., Pflaumann, U., & Sarnthein, M. (1986). Molecular stratigraphy: a new tool for climatic assessment. Nature, 320(6058), 129-133.

Bruch, A. A., Utescher, T., & Mosbrugger, V. (2011). Precipitation patterns in the Miocene of Central Europe and the development of continentality. Palaeogeography, Palaeoclimatology, Palaeoecology, 304(3), 202-211.

Boccaletti, G., Pacanowski, R. C., George, S., Philander, H., & Fedorov, A. V. (2004). The thermal structure of the upper ocean. Journal of physical oceanography, 34(4), 888-902.

Brierley, C. M., Fedorov, A. V., Liu, Z., Herbert, T. D., Lawrence, K. T., & LaRiviere, J. P. (2009). Greatly expanded tropical warm pool and weakened Hadley circulation in the early Pliocene. Science, 323(5922), 1714-1718.

Brochier-Armanet, C., Boussau, B., Gribaldo, S., & Forterre, P. (2008). Mesophilic Crenarchaeota: proposal for a third archaeal phylum, the Thaumarchaeota. Nature Reviews Microbiology, 6(3), 245-252.

Cerling, T. E., Harris, J. M., MacFadden, B. J., Leakey, M. G., Quade, J., Eisenmann, V., & Ehleringer, J. R. (1997). Global vegetation change through the Miocene/Pliocene boundary. Nature, 389(6647), 153-158.

Chen, W., Mohtadi, M., Schefuß, E., & Mollenhauer, G. (2014). Organic-geochemical proxies of sea surface temperature in surface sediments of the tropical eastern Indian Ocean. Deep Sea Research Part I: Oceanographic Research Papers, 88, 17-29.

Conte, M. H., Eglinton, G., & Madureira, L. A. (1992). Long-chain alkenones and alkyl alkenoates as palaeotemperature indicators: their produc tion, flux and early sedimentary diagenesis in the Eastern North Atlantic. Organic Geochemistry, 19(1-3), 287-298.

Conte, M. H., Thompson, A., Lesley, D., & Harris, R. P. (1998). Genetic and physiological influences on the alkenone/alkenoate versus growth temperature relationship in Emiliania huxleyi and Gephyrocapsa oceanica. Geochimica et Cosmochimica Acta, 62(1), 51-68.

Dowsett, H., Robinson, M., Haywood, A., Salzmann, U., Hill, D., Sohl, L., ... & Stoll, D. (2010). The PRISM3D paleoenvironmental reconstruction.

Dupont, L. M., Rommerskirchen, F., Mollenhauer, G., & Schefuß, E. (2013). Miocene to Pliocene changes in South African hydrology and vegetation in relation to the expansion of C 4 plants. Earth and Planetary Science Letters, 375, 408-417.

Fedorov, A. V., Brierley, C. M., Lawrence, K. T., Liu, Z., Dekens, P. S., & Ravelo, A. C. (2013). Patterns and mechanisms of early Pliocene warmth. Nature, 496(7443), 43-49.

Fedorov, A. V., Pacanowski, R. C., Philander, S. G., & Boccaletti, G. (2004). The effect of salinity on the wind-driven circulation and the thermal structure of the upper ocean. Journal of physical oceanography, 34(9), 1949-1966.

Flower, B. P., & Kennett, J. P. (1994). The middle Miocene climatic transition: East Antarctic ice sheet development, deep ocean circulation and global carbon cycling. Palaeogeography, palaeoclimatology, palaeoecology, 108(3-4), 537-555.

Foster, G. L., Lear, C. H., & Rae, J. W. (2012). The evolution of pCO 2, ice volume and climate during the middle Miocene. Earth and Planetary Science Letters, 341, 243-254.

Gent, P. R., Danabasoglu, G., Donner, L. J., Holland, M. M., Hunke, E. C., Jayne, S. R., ... & Worley, P. H. (2011). The community climate system model version 4. Journal of Climate, 24(19), 4973-4991.

Goldner, A., Herold, N., & Huber, M. (2014). The Challenge of Simulating the Warmth of the Mid-Miocene Climatic Optimun in CESM1. Climate of the Past.

Groeneveld, J., Nürnberg, D., Tiedemann, R., Reichart, G. J., Steph, S., Reuning, L., ... & Mason, P. (2008). Foraminiferal Mg/Ca increase in the Caribbean during the Pliocene: Western Atlantic Warm Pool formation, salinity influence, or diagenetic overprint?. Geochemistry, Geophysics, Geosystems, 9(1).

Gu, G., & Adler, R. F. (2004). Seasonal evolution and variability associated with the West African monsoon system. Journal of climate, 17(17), 3364-3377.

Hardman-Mountford, N. J., & McGlade, J. M. (2003). Seasonal and interannual variability of oceanographic processes in the Gulf of Guinea: an investigation using AVHRR sea surface temperature data. International Journal of Remote Sensing, 24(16), 3247-3268.

Haug, G. H., & Tiedemann, R. (1998). Effect of the formation of the Isthmus of Panama on Atlantic Ocean thermohaline circulation. Nature, 393(6686), 673-676.

Haug, G. H., Tiedemann, R., Zahn, R., & Ravelo, A. C. (2001). Role of Panama uplift on oceanic freshwater balance. Geology, 29(3), 207-210.

Haywood, A. M., Dowsett, H. J., Robinson, M. M., Stoll, D. K., Dolan, A. M., Lunt, D. J., ... & Chandler, M. A. (2011). Pliocene Model Intercomparison Project (PlioMIP): experimental design and boundary conditions (experiment 2).

Haywood, A. M., Hill, D. J., Dolan, A. M., Otto-Bliesner, B. L., Bragg, F., Chan, W. L., ... & Kamae, Y. (2013). Large-scale features of Pliocene climate: results from the Pliocene Model Intercomparison Project. Climate of the Past, 9(1), 191.

Herbert, T. D., Lawrence, K. T., Tzanova, A., Peterson, L. C., Caballero-Gill, R., & Kelly, C. S. (2016). Late Miocene global cooling and the rise of modern ecosystems. Nature Geoscience.

Herfort, L., Schouten, S., Boon, J. P., & Damsté, J. S. S. (2006). Application of the TEX 86 temperature proxy to the southern North Sea. Organic Geochemistry, 37(12), 1715-1726.

Hernández-Sánchez, M. T., Woodward, E. M. S., Taylor, K. W. R., Henderson, G. M., & Pancost, R. D. (2014). Variations in GDGT distributions through the water column in the South East Atlantic Ocean. Geochimica et Cosmochimica Acta, 132, 337-348.

Ho, S. L., & Laepple, T. (2016). Flat meridional temperature gradient in the early Eocene in the subsurface rather than surface ocean. Nature Geoscience, 9(8), 606-610.

Hopmans, E. C., Schouten, S., & Damsté, J. S. S. (2016). The effect of improved chromatography on GDGT-based palaeoproxies. Organic Geochemistry, 93, 1-6.

Hopmans, E. C., Weijers, J. W., Schefuß, E., Herfort, L., Damsté, J. S. S., & Schouten, S. (2004). A novel proxy for terrestrial organic matter in sediments based on branched and isoprenoid tetraether lipids. Earth and Planetary Science Letters, 224(1), 107-116.

Houghton, R. W. (1976). Circulation and hydrographic structure over the Ghana continental shelf during the 1974 upwelling. Journal of Physical Oceanography, 6(6), 909-924.

Huguet, C., Schimmelmann, A., Thunell, R., Lourens, L. J., Sinninghe Damsté, J. S., & Schouten, S. (2007). A study of the TEX86 paleothermometer in the water column and sediments of the Santa Barbara Basin, California. Paleoceanography, 22(3).

Ibaraki, M. (1997). Closing of the Central American Seaway and Neogene coastal upwelling along the Pacific coast of South America. Tectonophysics, 281(1-2), 99-104.

Jouanno, J., Marin, F., Du Penhoat, Y., Molines, J. M., & Sheinbaum, J. (2011). Seasonal modes of surface cooling in the Gulf of Guinea. Journal of Physical Oceanography, 41(7), 1408-1416.

Kamikuri, S. I., Motoyama, I., Nishi, H., & Iwai, M. (2009). Evolution of Eastern Pacific Warm Pool and upwelling processes since the middle Miocene based on analysis of radiolarian assemblages: Response to Indonesian and Central American Seaways. Palaeogeography, Palaeoclimatology, Palaeoecology, 280(3), 469-479.

Karner, M. B., DeLong, E. F., & Karl, D. M. (2001). Archaeal dominance in the mesopelagic zone of the Pacific Ocean. Nature, 409(6819), 507-510.

Keigwin, L. (1982). Isotopic paleoceanography of the Caribbean and East Pacific: role of Panama uplift in late Neogene time. Science, 217(4557), 350-353.

Kim, J. H., Schouten, S., Hopmans, E. C., Donner, B., & Damsté, J. S. S. (2008). Global sediment core-top calibration of the TEX 86 paleo thermometer in the ocean. Geochimica et Cosmochimica Acta, 72(4), 1154-1173.

Kim, J. H., Schouten, S., Rodrigo-Gámiz, M., Rampen, S., Marino, G., Huguet, C., ... & Sangiorgi, F. (2015). Influence of deep-water derived isoprenoid tetraether lipids on the paleothermometer in the Mediterranean Sea. Geochimica et Cosmochimica Acta, 150, 125-141.

Kim, J. H., Van der Meer, J., Schouten, S., Helmke, P., Willmott, V., Sangiorgi, F., ... & Damsté, J. S. S. (2010). New indices and calibrations derived from the distribution of crenarchaeal isoprenoid tetraether lipids: Implications for past sea surface temperature reconstructions. Geochimica et Cosmochimica Acta, 74(16), 4639-4654.

Kirby, M. X., Jones, D. S., & MacFadden, B. J. (2008). Lower Miocene stratigraphy along the Panama Canal and its bearing on the Central American Peninsula. PLoS One, 3(7), e2791.

LaRiviere, J. P., Ravelo, A. C., Crimmins, A., Dekens, P. S., Ford, H. L., Lyle, M., & Wara, M. W. (2012). Late Miocene decoupling of oceanic warmth and atmospheric carbon dioxide forcing. Nature, 486(7401), 97-100.

Larsen, H. C., Saunders, A. D., Clift, P. D., Beget, J., Wei, W., Spezzaferri, S., ... & Fram, M. S. (1994). Seven million years of glaciation in Greenland. Science-AAAS-Weekly Paper Edition-including Guide to Scientific Information, 264(5161), 952-954.

Lee, K. E., Kim, J. H., Wilke, I., Helmke, P., & Schouten, S. (2008). A study of the alkenone, TEX86, and planktonic foraminifera in the Benguela Upwelling System: Implications for past sea surface temperature estimates. Geochemistry, Geophysics, Geosystems, 9(10).

Lewis, A. R., Marchant, D. R., Ashworth, A. C., Hedenäs, L., Hemming, S. R., Johnson, J. V., ... & Willenbring, J. K. (2008). Mid-Miocene cooling and the extinction of tundra in continental Antarctica. Proceedings of the National Academy of Sciences, 105(31), 10676-10680.

Lopes dos Santos, R. A., Prange, M., Castañeda, I. S., Schefuß, E., Mulitza, S., Schulz, M., ... & Schouten, S. (2010). Glacial–interglacial variability in Atlantic meridional overturning circulation and thermocline adjustments in the tropical North Atlantic. Earth and Planetary Science Letters, 300(3), 407-414.

Lunt, D. J., Valdes, P. J., Haywood, A., & Rutt, I. C. (2008). Closure of the Panama Seaway during the Pliocene: implications for climate and Northern Hemisphere glaciation. Climate Dynamics, 30(1), 1-18.

Marchal, E., & Picaut, J. (1977). Répartition et abondance évaluées par échointégration des poissons du plateau ivoiro-ghanéen en relation avec les upwellings locaux.

Maier-Reimer, E., Mikolajewicz, U., & Crowley, T. (1990). Ocean general circulation model sensitivity experiment with an open Central American Isthmus. Paleoceanography, 5(3), 349-366.

Marlowe, I. T., Brassell, S. C., Eglinton, G., & Green, J. C. (1990). Long-chain alkenones and alkyl alkenoates and the fossil coccolith record of marine sediments. Chemical Geology, 88(3-4), 349-375.

Marlowe, I. T., Green, J. C., Neal, A. C., Brassell, S. C., Eglinton, G., & Course, P. A. (1984). Long chain (n-C37–C39) alkenones in the Prymnesio phyceae. Distribution of alkenones and other lipids and their taxo nomic significance. British Phycological Journal, 19(3), 203-216.

Mascle, J., Lohmann, G.P., Clift, P.D., et al., 1996. Proc. ODP, Init. Repts., 159: College Station, TX (Ocean Drilling Program)

Montes, C., Cardona, A., Jaramillo, C., Pardo, A., Silva, J. C., Valencia, V., ... & Niño, H. (2015). Middle Miocene closure of the Central American seaway. Science, 348(6231), 226-229.

Moore, D., Hisard, P., McCreary, J., Merle, J., O'Brien, J., Picaut, J., ... & Wunsch, C. (1978). Equatorial adjustment in the eastern Atlantic. Geophysical Research Letters, 5(8), 637-640.

Müller, P. J., Kirst, G., Ruhland, G., Von Storch, I., & Rosell-Melé, A. (1998). Calibration of the alkenone paleotemperature index U 37 K′ based on core-tops from the eastern South Atlantic and the global ocean (60 N-60 S). Geochimica et Cosmochimica Acta, 62(10), 1757-1772.

Norris, R. D. (1998). Miocene-Pliocene surface-water hydrography of the eastern equatorial Atlantic. In Proceedings-Ocean Drilling Program Scientific Results (pp. 539-556). National Science Foundation.

Pagani, M., Arthur, M. A., & Freeman, K. H. (1999). Miocene evolution of atmospheric carbon dioxide. Paleoceanography, 14(3), 273-292.

Pancost, R. D., van Geel, B., Baas, M., & Damsté, J. S. S. (2000). δ13C values and radiocarbon dates of microbial biomarkers as tracers for carbon recycling in peat deposits. Geology, 28(7), 663-666.

Picaut, J. (1983). Propagation of the seasonal upwelling in the eastern equatorial Atlantic. Journal of Physical Oceanography, 13(1), 18-37.

Pitcher, A., Wuchter, C., Siedenberg, K., Schouten, S., & Sinninghe Damsté, J. S. (2011). Crenarchaeol tracks winter blooms of ammonia-oxidizing Thaumarchaeota in the coastal North Sea. Limnology and Oceanography, 56(6), 2308-2318.

Prahl, F. G., & Wakeham, S. G. (1987). Calibration of unsaturation patterns in long-chain ketone compositions for palaeotemperature assess ment. Nature, 330(6146), 367-369.

Rahmstorf, S. (2002). Ocean circulation and climate during the past 120,000 years. Nature, 419(6903), 207-214.

Rampen, S. W., Schouten, S., Koning, E., Brummer, G. J. A., & Damsté, J. S. S. (2008). A 90 kyr upwelling record from the northwestern Indian Ocean using a novel long-chain diol index. Earth and Planetary Science Letters, 276(1), 207-213.

Ravelo, A. C., & Fairbanks, R. G. (1992). Oxygen isotopic composition of multiple species of planktonic foraminifera: Recorders of the modern photic zone temperature gradient. Paleoceanography, 7(6), 815-831.

Rommerskirchen, F., Condon, T., Mollenhauer, G., Dupont, L., & Schefuß, E. (2011). Miocene to Pliocene development of surface and subsurface temperatures in the Benguela Current system. Paleoceanography, 26(3).

Rosenbloom, N. A., Otto-Bliesner, B. L., Brady, E. C., & Lawrence, P. J. (2013). Simulating the mid-Pliocene Warm Period with the CCSM4 model. Geoscientific Model Development, 6(2), 549-561.

Roy, C. (1995). The Côte d'Ivoire and Ghana coastal upwelling dynamics and changes.

Schouten, S., Hopmans, E. C., Pancost, R. D., & Damsté, J. S. S. (2000). Widespread occurrence of structurally diverse tetraether membrane lipids: evidence for the ubiquitous presence of low-temperature relatives of hyperthermophiles. Proceedings of the National Academy of Sciences, 97(26), 14421-14426.

Schouten, S., Hopmans, E. C., Schefuß, E., & Damste, J. S. S. (2002). Distri butional variations in marine crenarchaeotal membrane lipids: a new tool for reconstructing ancient sea water temperatures?. Earth and Planetary Science Letters, 204(1), 265-274.

Seki, O., Schmidt, D. N., Schouten, S., Hopmans, E. C., Sinninghe Damsté, J. S., & Pancost, R. D. (2012). Paleoceanographic changes in the Eastern Equatorial Pacific over the last 10 Myr. Paleoceanography, 27(3).

Sepulchre, P., Arsouze, T., Donnadieu, Y., Dutay, J. C., Jaramillo, C., Le Bras, J., ... & Waite, A. J. (2014). Consequences of shoaling of the Central American Seaway determined from modeling Nd isotopes. Paleoceanography, 29(3), 176-189.

Sinninghe Damsté, J. S.., Hopmans, E. C., Pancost, R. D., Schouten, S., & Geenevasen, J. A. (2000). Newly discovered non-isoprenoid glycerol dialkyl glycerol tetraether lipids in sediments. Chemical Communications, (17), 1683-1684.

Sinninghe Damsté, J. S., Rijpstra, W. I. C., Hopmans, E. C., Prahl, F. G., Wakeham, S. G., & Schouten, S. (2002). Distribution of membrane lipids of planktonic Crenarchaeota in the Arabian Sea. Applied and Environmental Microbiology, 68(6), 2997-3002.

Smith, R., Jones, P., Briegleb, B., Bryan, F., Danabasoglu, G., Dennis, J., ... & Hecht, M. (2010). The parallel ocean program (POP) reference manual ocean component of the community climate system model (CCSM) and community earth system model (CESM). Rep. LAUR-01853, 141.

Steph, S., Tiedemann, R., Prange, M., Groeneveld, J., Nürnberg, D., Reuning, L., ... & Haug, G. H. (2006). Changes in Caribbean surface hydrography during the Pliocene shoaling of the Central American Seaway. Paleoceanography, 21(4).

Sultan, B., & Janicot, S. (2003). The West African monsoon dynamics. Part II: The "preonset" and "onset" of the summer monsoon. Journal of climate, 16(21), 3407-3427.

Talley, L. D. (2011). Descriptive physical oceanography: an introduction. Academic press.

Taylor, K. W., Huber, M., Hollis, C. J., Hernandez-Sanchez, M. T., & Pancost, R. D. (2013). Re-evaluating modern and Palaeogene GDGT distributions: Implications for SST reconstructions. Global and Planetary Change, 108, 158-174.

Taylor, K. E., Stouffer, R. J., & Meehl, G. A. (2012). An overview of CMIP5 and the experiment design. Bulletin of the American Meteorological Society, 93(4), 485-498.

Tierney, J. E., & Tingley, M. P. (2014). A Bayesian, spatially-varying calibration model for the TEX 86 proxy. Geochimica et Cosmochimica Acta, 127, 83-106.

Turich, C., Freeman, K. H., Bruns, M. A., Conte, M., Jones, A. D., & Wakeham, S. G. (2007). Lipids of marine Archaea: Patterns and provenance in the water-column and sediments. Geochimica et Cosmochimica Acta, 71(13), 3272-3291.

Vallé, F., Westerhold, T., & Dupont, L. M. (2016). Orbital-driven environmental changes recorded at ODP Site 959 (eastern equatorial Atlantic) from the Late Miocene to the Early Pleistocene. International Journal of Earth Sciences, 1-14.

Verstraete, J. M. (1992). The seasonal upwellings in the Gulf of Guinea. Progress in Oceanography, 29(1), 1-60.

Volkman, J. K., Eglinton, G., Corner, E. D. S., & Sargent, J. R. (1980). Novel unsaturated straight-chain C37□ C39 methyl and ethyl ketones in marine sediments and a coccolithophore Emiliania huxleyi. Physics and Chemistry of the Earth, 12, 219-227.

Wakeham, S. G., Hopmans, E. C., Schouten, S., & Damsté, J. S. S. (2004). Archaeal lipids and anaerobic oxidation of methane in euxinic water columns: a comparative study of the Black Sea and Cariaco Basin. Chemical Geology, 205(3), 427-442.

Wakeham, S. G., Peterson, M. L., Hedges, J. I., & Lee, C. (2002). Lipid biomarker fluxes in the Arabian Sea, with a comparison to the equatorial Pacific Ocean. Deep Sea Research Part II: Topical Studies in Oceanography, 49(12), 2265-2301.

Wang, Y., Cerling, T. E., & MacFadden, B. J. (1994). Fossil horses and carbon isotopes: new evidence for Cenozoic dietary, habitat, and ecosystem changes in North America. Palaeogeography, Palaeoclimatology, Palaeoecology, 107(3-4), 269-279.

Weijers, J. W., Schouten, S., Spaargaren, O. C., & Damsté, J. S. S. (2006). Occurrence and distribution of tetraether membrane lipids in soils: implications for the use of the TEX 86 proxy and the BIT index. Organic Geochemistry, 37(12), 1680-1693.

Weijers, J. W., Schouten, S., van der Linden, M., van Geel, B., & Damsté, J. S. S. (2004). Water table related variations in the abundance of intact archaeal membrane lipids in a Swedish peat bog. FEMS Microbiology Letters, 239(1), 51-56.

Wuchter, C., Abbas, B., Coolen, M. J., Herfort, L., van Bleijswijk, J., Timmers, P., ... & Schouten, S. (2006). Archaeal nitrification in the ocean. Proceedings of the National Academy of Sciences, 103(33), 12317-12322.

Wuchter, C., Schouten, S., Coolen, M. J., & Sinninghe Damsté, J. S. (2004). Temperature-dependent variation in the distribution of tetraether membrane lipids of marine Crenarchaeota: Implications for TEX86 paleothermometry. Paleoceanography, 19(4).

Wuchter, C., Schouten, S., Wakeham, S. G., & Sinninghe Damsté, J. S. (2005). Temporal and spatial variation in tetraether membrane lipids of marine Crenarchaeota in particulate organic matter: implications for TEX86 paleothermometry. Paleoceanography, 20(3).

Wuchter, C., Schouten, S., Wakeham, S. G., & Sinninghe Damsté, J. S. (2006). Archaeal tetraether membrane lipid fluxes in the northeastern Pacific and the Arabian Sea: implications for TEX86 paleothermometry. Paleoceanography, 21(4).

You, Y., Huber, M., Müller, R. D., Poulsen, C. J., & Ribbe, J. (2009). Simulation of the middle Miocene climate optimum. Geophysical Research Letters, 36(4).

Zachos, J. C., Dickens, G. R., & Zeebe, R. E. (2008). An early Cenozoic perspective on greenhouse warming and carbon-cycle dynamics. Nature, 451(7176), 279-283.

Zachos, J., Pagani, M., Sloan, L., Thomas, E., & Billups, K. (2001). Trends, rhythms, and aberrations in global climate 65 Ma to present. Science, 292(5517), 686-693.

Zhang, Y. G., Zhang, C. L., Liu, X. L., Li, L., Hinrichs, K. U., & Noakes, J. E. (2011). Methane Index: a tetraether archaeal lipid biomarker indicator for detecting the instability of marine gas hydrates. Earth and Planetary Science Letters, 307(3), 525-534.

SUPPLEMENTARY FIGURES

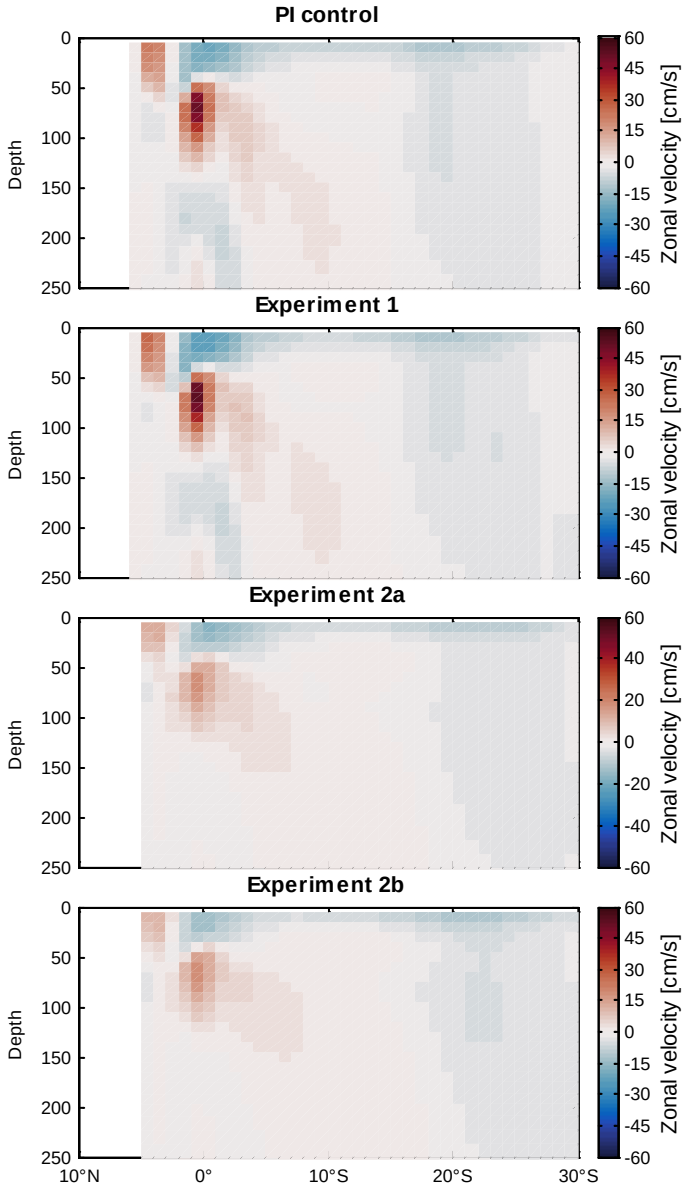

Supplementary Figure 1. Zonal velocities at 5°W (for line see Fig. 4c). Red (blue) colors indicate an eastward (westward) flow.

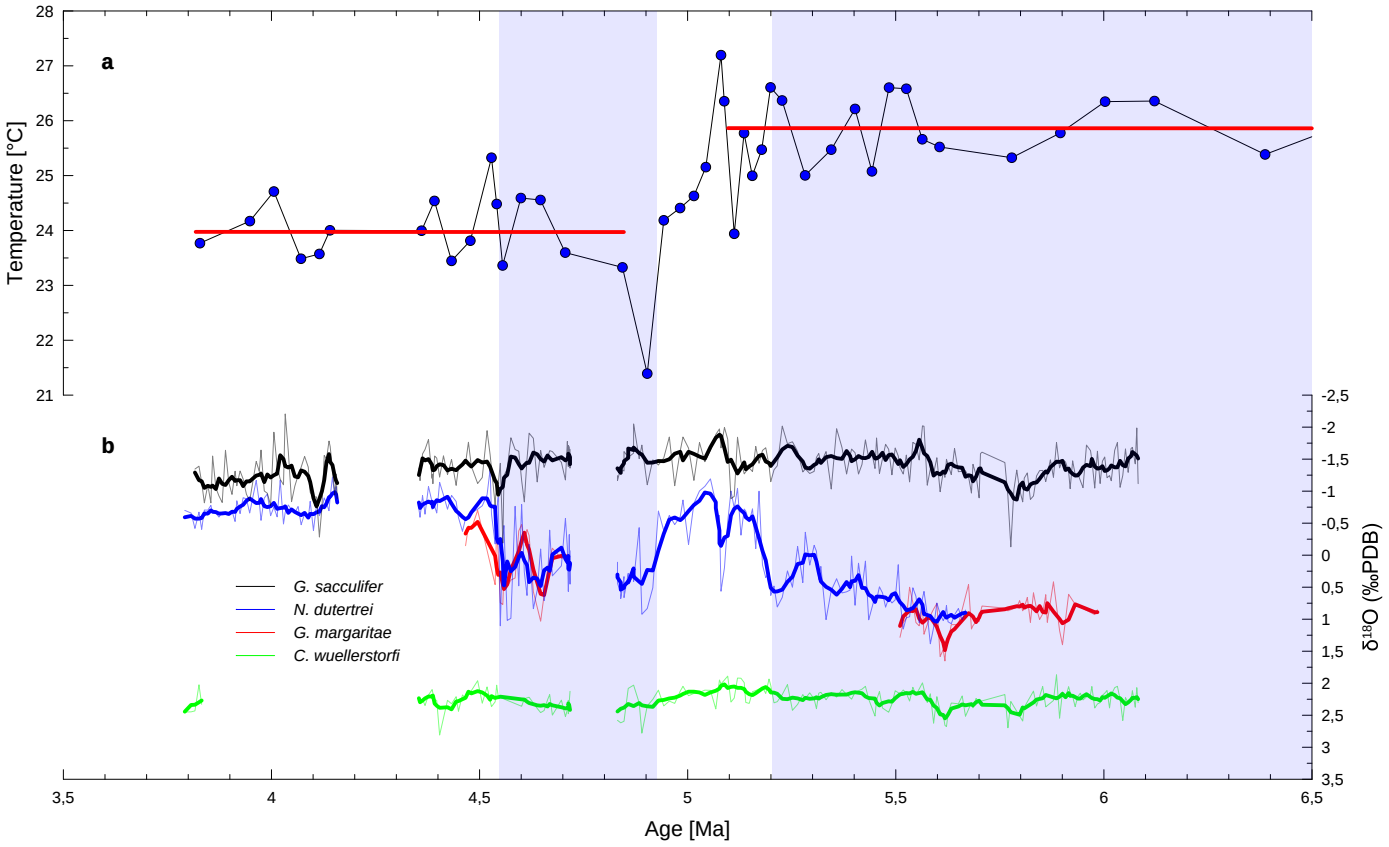

Supplementary Figure 2. a. TEX_{86}^{H} SST evolution at ODP Site 959 from 6.5-3.7 Ma. The red lines indicate the average SST before 5.1 Ma and after 4.8 Ma. **b.** $\delta^{18}O$ values of surface (*G. sacculifer*), subsurface (*N. dutertrei* and *G. margaritae*) and bottom (*C. wuellerstorfi*) dwelling foraminifera.